ENT Updates
https://ojs.ukscip.com/index.php/ENTU

Article

Ferroptosis-Related Gene *BCL2L10* is Linked to Prognosis in Head and Neck Squamous Cell Carcinoma

Guancheng Liu [1], Yulin Chen [2], Xingnong Xu [3,4], Yudi Zhu [1], Xing Ye [5,*] and Shichao Liu [2,*]

[1] International Cultural and Educational College, Northeast Agricultural University, Harbin 150030, China
[2] College of Veterinary Medicine, Northeast Agricultural University, Harbin 150030, China
[3] School of Pharmacy, East China University of Science and Technology, Shanghai 200237, China
[4] Department of Pharmacy, Yancheng Third People's Hospital, Yancheng 224000, China
[5] Department of Pharmacy, Taizhou Second People's Hospital, Taizhou 225500, China
[*] Correspondence: LSC10251025@163.com (S.L.); 1299095445@qq.com (X.Y.)

Received: 28 July 2025; **Revised:** 13 August 2025; **Accepted:** 27 August 2025; **Published:** 8 September 2025

Abstract: Ferroptosis, an iron-dependent form of regulated cell death, is driven by the accumulation of lipid peroxides and shaped by mitochondrial metabolism. However, the role of BCL2L10 (B-cell lymphoma 2-like 10)—a gene previously implicated in ferroptosis—in affecting the immune microenvironment and clinical progression of head and neck squamous cell carcinoma (HNSCC) remains unclear. Using RNA-seq data from The Cancer Genome Atlas (TCGA), we compared BCL2L10 expression in HNSCC tumors and matched normal tissues and corroborated the results with immunohistochemistry images from the Human Protein Atlas (HPA). Logistic regression and Kaplan–Meier analyses were then applied to assess the relationship between BCL2L10 levels and clinical outcomes. The protein–protein interaction network centered on BCL2L10 was constructed with the STRING database, and the immunological relevance of BCL2L10 was explored through three complementary approaches: Gene Ontology (GO) annotation, gene set enrichment analysis (GSEA), and single-sample GSEA (ssGSEA). BCL2L10 mRNA levels were markedly higher in HNSCC tumors than in adjacent normal tissues. Nevertheless, univariate survival analysis revealed no significant difference in overall survival between patients with high versus low BCL2L10 expression ($p > 0.05$). Mechanistically, BCL2L11 emerged as a key interactor of BCL2L10, and tumors overexpressing BCL2L10 exhibited reduced infiltration by immune cells. Overall, elevated BCL2L10 expression in HNSCC is associated with an unfavorable prognosis and an immunosuppressive tumor microenvironment.

Keywords: BCL2L10; Head and Neck Squamous Cell Carcinoma; Immune Infiltration

1. Introduction

Head and neck squamous cell carcinoma (HNSCC) is the sixth most common malignant tumor globally, accounting for more than 90% of all head and neck malignancies. Its occurrence is closely related to factors such as smoking, excessive alcohol consumption, and human papillomavirus (HPV) infection [1]. HNSCC has high invasiveness, easily leads to regional lymph node metastasis, and has a high recurrence rate after treatment, with a 5-year survival rate of only 40%–60% [2]. Currently, the first-line treatment strategy for HNSCC depends on tumor staging and location, primarily including surgical resection, radiotherapy, chemotherapy, and targeted therapy [3,4]. However,

existing therapies still face numerous challenges, including treatment resistance and severe toxic side effects. Additionally, the immunosuppressive characteristics of the tumor microenvironment (TME), tumor heterogeneity, and epigenetic changes are key reasons for treatment failure [5]. In recent years, research on the treatment of HNSCC has made significant progress. New immunotherapies, such as bispecific antibodies and personalized tumor vaccines, and targeted drugs, such as EGFR and PI3K/mTOR pathway inhibitors, have shown good anti-tumor activity in clinical trials [6,7]. Moreover, the application of AI-based precision medicine strategies and liquid biopsy technology provides new directions for the early diagnosis and dynamic monitoring of HNSCC [8,9]. Future research should focus on exploring reliable biomarkers and developing new targeted drugs aimed at resistance mechanisms to improve survival and prognosis for HNSCC [10].

Ferroptosis is an iron-dependent form of programmed cell death, with its core mechanisms involving the inhibition of glutathione peroxidase 4 (GPX4) activity, accumulation of lipid peroxides, and dysregulation of iron metabolism [11]. Unlike other forms of cell death, such as apoptosis and necrosis, ferroptosis exhibits unique morphological and biochemical characteristics, including mitochondrial condensation, lipid peroxidation, and a reactive oxygen species (ROS) burst [12]. In recent years, ferroptosis has garnered significant attention for its role in cancer treatment, as it can selectively kill tumor cells by targeting their antioxidant defense systems [13]. BCL2L10 is a member of the BCL-2 protein family and has anti-apoptotic functions. It promotes cell survival by inhibiting the mitochondrial apoptosis pathway dependent on BAX/BAK [14]. Research shows that BCL2L10 is highly expressed in various cancers and is associated with chemotherapy resistance and poor prognosis [15]. In HNSCC, the overexpression of BCL2L10 may contribute to disease progression by inhibiting apoptosis and promoting tumor cell proliferation [16]. Recent studies have found that BCL2L10 may influence the fate of tumor cells by regulating ferroptosis. For example, BCL2L10 can affect ferroptosis sensitivity by modulating iron metabolism-related proteins (such as TFR1, FTH1) or antioxidant pathways [17,18]. Additionally, the interaction between BCL2L10 and p53 may further regulate the expression of genes related to ferroptosis [19]. Nonetheless, the biological function of BCL2L10 in HNSCC remains to be elucidated.

This investigation utilized transcriptomic and clinical datasets from GEO, TCGA, and HPA to examine correlations between BCL2L10 expression levels, clinicopathological parameters, and survival outcomes in HNSCC patients. Subsequently, we extracted datasets from TIMER and GEPIA to analyze potential correlations between BCL2L10 expression patterns, immune cell infiltration levels, and related immunological gene signatures. Protein–protein interaction networks involving BCL2L10 were subsequently constructed using the STRING database. Higher *BCL2L10* gene levels were linked to reduced immune cell invasion in HNSCC tissue, indicating a poor prognosis. Therefore, it is reasonable that *BCL2L10* gene defects might strengthen the anti-tumor immunity effect in HNSCC. Targeted combined immunotherapy, associated with BCL2L10, may be a feasible treatment option in HNSCC.

2. Materials and Methods

2.1. Data Source

As a major component of the NCI's cancer genomics program, the TCGA systematically catalogs clinical and molecular data across diverse malignancies. Our investigation specifically retrieved HNSCC-related clinical annotations and transcriptomic data (RNA-seq) from this curated database. The fragments per kilobase per million mapped fragments (FPKM) method, as implemented in HTSeq, was utilized to ascertain transcript expression levels. Additionally, for further analysis, the RNA-Seq gene expression level 3 HTSeqFPKM data from patients with HNSCC and the corresponding clinical data were converted into transcripts per million (TPM) reads. Since the database is publicly accessible, no approval from the local ethics committee was deemed necessary.

2.2. HPA Datasets

The HPA compiles comprehensive transcriptomic and proteomic data from a variety of human samples, encompassing tissue, cellular, and pathological atlases. Currently, the platform archives cellular localization data across 44 normal human tissues and 20 high-incidence malignancies. The database further encompasses immunohistochemical protein expression profiles for both malignant and non-malignant human tissue specimens.

2.3. Statistical Evaluation of Clinical Outcomes, Alongside the Creation and Appraisal of Predictive Models

The analysis of prognostic factors, including overall survival (OS), disease-specific survival (DSS), and progression-free survival (PFS), was conducted using clinical data sourced from the TCGA through the module for deriving clinical insights available on the Xiantao platform. The Cox proportional hazards regression model and Kaplan–Meier survival curves were employed in these assessments. The BCL2L10 expression groups were dichotomized using median cutoff values. Associations with clinicopathological features were evaluated through Wilcoxon rank-sum tests and logistic regression modeling. The impact of *BCL2L10* gene expression on survival and other clinical variables was assessed using a Cox regression analysis. Statistical significance was set at $p < 0.05$. The outputs from the Cox model were integrated with significant multivariate predictors to generate survival estimates for 1, 3, and 5 years. The prediction accuracy was assessed using calibration plots, where perfect concordance aligns with the 45° reference line.

2.4. In-Depth Investigation of Protein–Protein Interactions

The STRING platform served as the primary analysis tool, offering extensively integrated and consolidated protein–protein interaction (PPI) data. After uploading the BCL2L10 expression data to STRING, we obtained information from the PPI network. The significance threshold was identified by a confidence score of 0.7 or higher.

2.5. Enrichment Profiling

Functional annotation of genes associated with BCL2L10 was performed through GO enrichment analysis utilizing clusterProfiler (v3.6.3) in R, examining three core ontology domains: cellular components (CC), molecular functions (MF), and biological processes (BP). Significance thresholds were set at enrichment coefficient > 1.5, minimum gene count > 3, and p-value < 0.01. Pathway analysis employed GSEA methodology with 1,000 genome permutations, considering pathways significant at FDR (false discovery rate) < 0.25 and adjusted $p < 0.05$. The findings were interpreted using NES (normalized enrichment scores) and corrected p-values, with visualization conducted through clusterProfiler [20].

2.6. Immunological Infiltration Profiling

In a study by Tao et al. [20], marker genes for 24 distinct immune cell types were identified. Tumor infiltration by these immune cells was evaluated using the ssGSEA method. The Spearman rank correlation model was employed to compare the levels of immune cell invasion within subgroups characterized by high versus low *BCL2L10* gene transcription, thereby assessing the relationship between BCL2L10 activity and immunocyte invasion. The Xiantao tool was utilized to analyze the connection between BCL2L10 expression and immune infiltration, as well as the correlation between immune cell levels and BCL2L10 expression subgroups. This included data on immune infiltration, Spearman correlation analysis via the Xiantao tool, and the Wilcoxon signed-rank test. We adopted the conventional 0.05 cutoff for determining significance.

2.7. Intergenic Association Analysis

GEPIA serves as a web-based tool that provides access to data from cancer types and health specimens sourced from TCGA and GTEx. It primarily centers on RNA-seq analysis. The platform includes 60,498 gene types and 198,619 isoform types. An investigation in GEPIA examined the interrelation between *BCL2L10* gene activity and various immune cell markers. *BCL2L10* gene expression is plotted on the x-axis, with relevant gene expression profiles plotted on the ordinate. Furthermore, TIMER data supported gene expression patterns strongly linked to BCL2L10 as observed in GEPIA. Statistical significance was set at a p-value less than 0.05.

3. Results

3.1. *BCL2L10* Gene Expression Exhibited an Increase in Tumors Relative to Normal Samples

Pan-cancer screening revealed BCL2L10 overexpression as a frequent oncogenic event (**Figure 1A**). TCGA analysis of 504 HNSCC/44 normal samples showed significantly elevated BCL2L10 transcripts in tumors (**Figure 1B**).

This upregulation was confirmed in tumor-adjacent tissue comparisons (43 pairs, **Figure 1C**). To verify the diagnostic potential of BCL2L10, we generated ROC curves comparing its expression in HNSCC versus (a) GTEx-normalized tissues and (b) adjacent non-cancerous tissues. The resulting AUC of 0.654 (95% CI: 0.591–0.717) suggests certain discriminative ability (**Figure 1D**). In HNSCC tissues, the expression of BCL2L10 protein was notably increased compared to normal tissue samples (**Figure 1E**). Similarly, HPA data demonstrated that BCL2L10 protein expression was increased in HNSCC compared to normal controls (**Figure 2**).

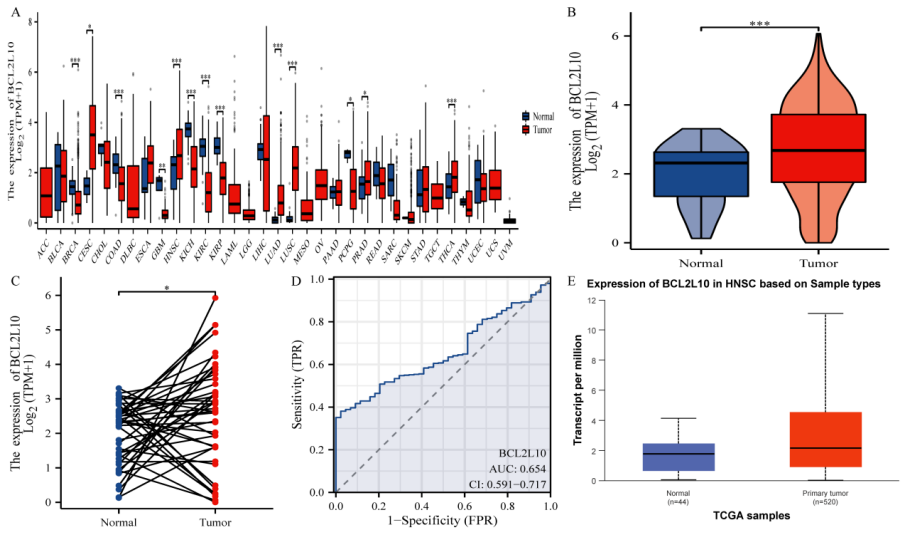

Figure 1. BCL2L10 oncogenic expression profile. (**A**) Pan-cancer vs. normal tissue comparison; (**B**) HNSCC tumor-adjacent tissue differential expression; (**C**) Matched tumor-normal paired analysis; (**D**) ROC curve analysis (GTEx controls vs. HNSCC samples); (**E**) Tumor-specific protein BCL2L10 upregulation.

Note: $*p < 0.05$, $**p < 0.01$, $***p < 0.001$, and ns: no statistical difference.

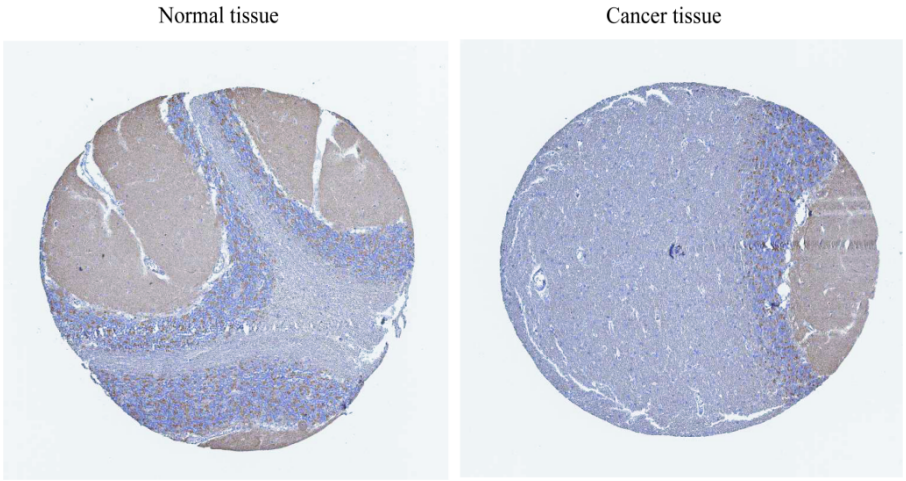

Figure 2. HPA data on BCL2L10 expression. An assessment of *BCL2L10* gene expression using the HPA showed that BCL2L10 protein levels were notably increased in HNSCC compared to normal control.

3.2. BCL2L10 Expression in Relation to Clinical Parameters

Using the Z-score criterion, the expression levels of BCL2L10 in tumor samples were determined. The HNSCC cohort was subsequently divided into expression-based subgroups (low/high). Kruskal–Wallis and Wilcoxon signed-rank examinations were applied to analyze the correlation between BCL2L10 expression and clinical indicators. Compared to the normal group, pathologic M stage, pathologic stage, clinical T stage, clinical N stage, clinical

M stage, clinical stage, primary therapy outcome (CR), and histologic grade showed significant positive correlations with elevated BCL2L10 levels (**Figures 3A–H**). Interestingly, univariate analysis demonstrated strong relationships between BCL2L10 expression and clinical indicators, particularly histological grade [odds ratio (OR) = 0.620 (0.409–0.941), $p = 0.025$] (**Table 1**). However, no statistically significant differences were found in the association with pathologic T stage [OR = 1.046 (0.717–1.526), $p = 0.816$], pathologic N stage [OR = 0.891 (0.603–1.316), $p = 0.561$], pathologic stage [OR = 0.944 (0.599–1.488), $p = 0.805$], age [OR = 0.833 (0.587–1.182), $p = 0.306$], or primary therapy outcome [OR = 1.442 (0.778–2.673), $p = 0.245$] (**Table 1**). Collectively, these results establish BCL2L10 as a potential biomarker for the occurrence of HNSCC.

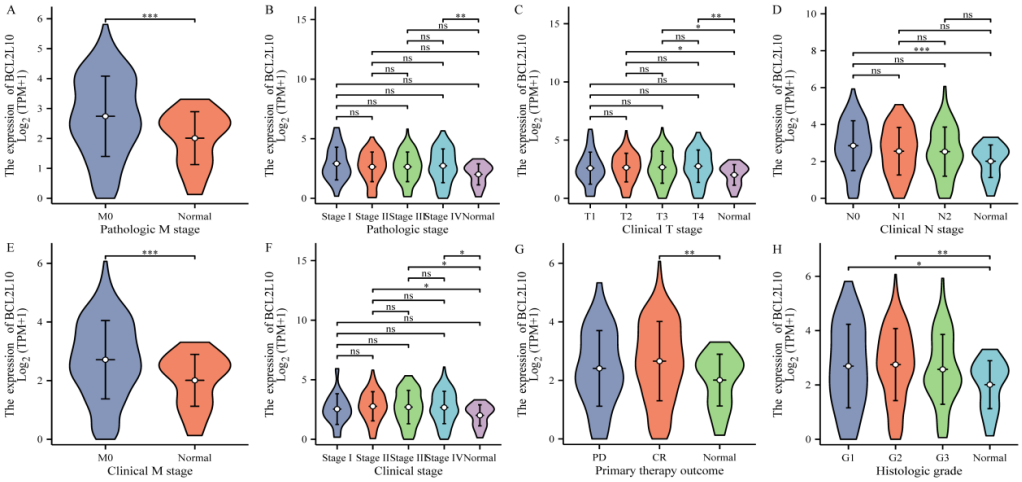

Figure 3. Correlation of BCL2L10 expression with clinical-pathological characteristics of HNSCC. (**A**) The correlation among BCL2L10 expression and pathologic M stage; (**B**) Pathologic stage; (**C**) Clinical T stage; (**D**) Clinical N stage; (**E**) Clinical M stage; (**F**) Clinical stage; (**G**) Primary therapy outcome; (**H**) Histologic grade.
Note: $^{*}p < 0.05$, $^{**}p < 0.01$, and $^{***}p < 0.001$.

Table 1. Logistic regression analysis of BCL2L10 expression.

Characteristics	Total (N)	OR (95% CI)	*p*-value
Pathologic T stage (T3 & T4 vs. T1 & T2)	448	1.046 (0.717–1.526)	0.816
Pathologic N stage (N1 & N2 vs. N0 & N3)	411	0.891 (0.603–1.316)	0.561
Pathologic M stage (M1 vs. M0)	189	65094951.2988 (0.000–Inf)	0.997
Pathologic stage (Stage III & Stage IV vs. Stage I & Stage II)	436	0.944 (0.599–1.488)	0.805
Age (> 60 vs. ≤ 60)	503	0.833 (0.587–1.182)	0.306
Primary therapy outcome (SD & CR vs. PD & PR)	419	1.442 (0.778–2.673)	0.245
Histologic grade (G3 & G4 vs. G1 & G2)	484	0.620 (0.409–0.941)	0.025

3.3. BCL2L10 Expression as a Prognostic Indicator in HNSCC

Survival analyses using TCGA data revealed no significant prognostic associations for BCL2L10 expression levels: OS (HR = 1.00, 95% CI 0.77–1.31, $p = 0.976$), DSS (HR = 0.96, 95% CI 0.68–1.36, $p = 0.818$), or PFS (HR = 0.88, 95% CI 0.66–1.17, $p = 0.386$) (**Figures 4A–C**). In this study, it was found that patients with HNSCC had increased risk scores and higher levels of BCL2L10 expression. Notably, those with higher risk scores also displayed significant BCL2L10 expression. The relationship between BCL2L10 expression and numerous cohorts was further verified. Specifically, BCL2L10 expression was discovered to be elevated in tumors with pathologic stage III–IV [HR = 1.839, 95% CI: 1.236–2.737, $p = 0.003$], pathologic T3 stage [HR = 2.592, 95% CI: 1.349–4.984, $p = 0.004$], pathologic T4 stage [HR = 2.347, 95% CI: 1.250–4.407, $p = 0.008$], pathologic N2–N3 stage [HR = 2.296, 95% CI: 1.686–3.127, $p < 0.001$], pathologic M1 stage [HR = 22.631, 95% CI: 2.830–180.948, $p = 0.003$] (**Figure 4D**). Moreover, a prognostic risk stratification tool for HNSCC was constructed, considering factors such as gender, pathologic TNM stages, age, pathologic stage, histologic grade, and BCL2L10 expression (**Figure 4E**). We also applied a calibration chart to assess the accuracy of the model's predictions (**Figure 4F**). BCL2L10 expression may offer a more

precise prediction of survival rates at 3 and 5 years. Generally, BCL2L10 expression has been linked to the prognosis of patients with HNSCC.

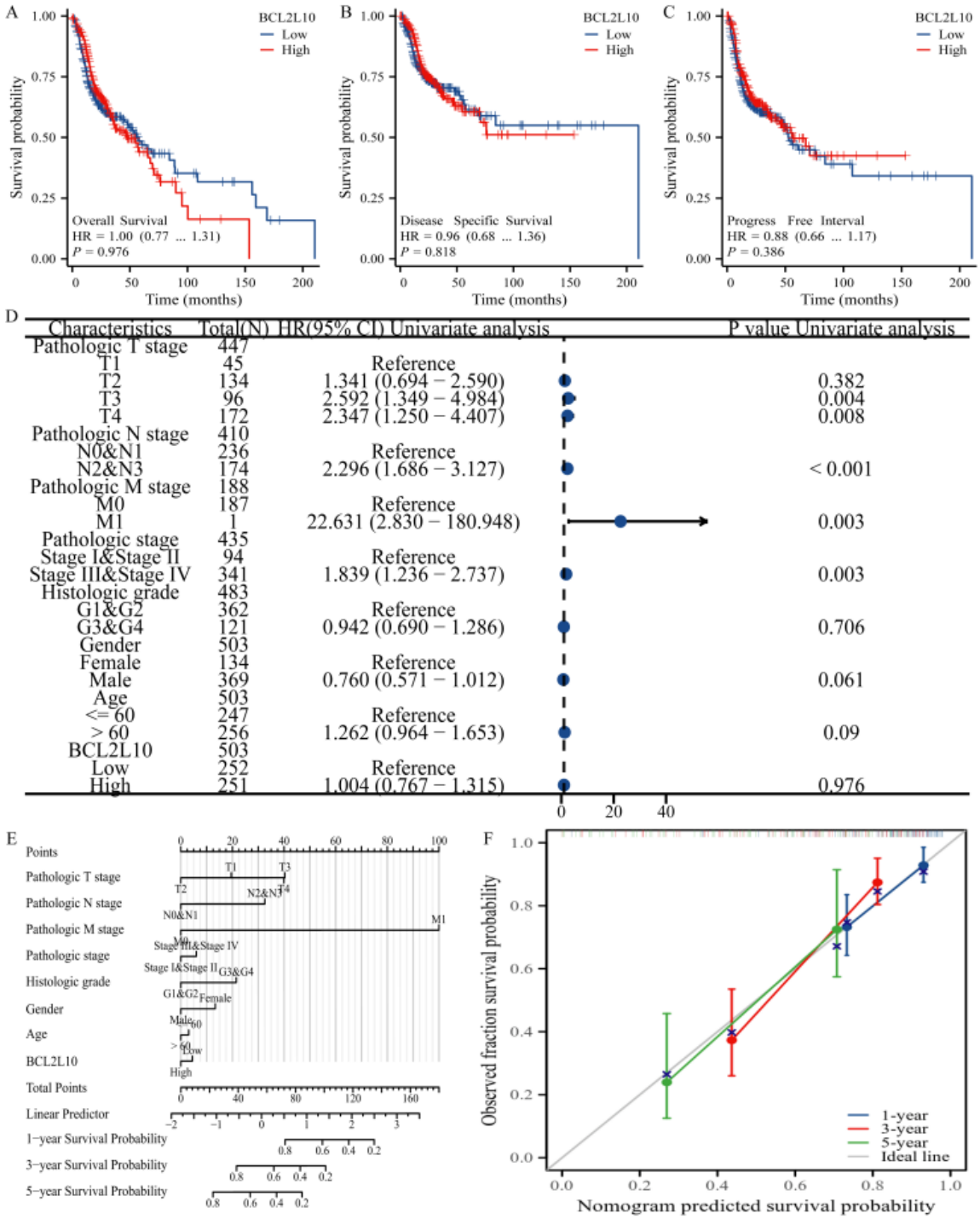

Figure 4. Prognostic analysis of BCL2L10 expression. Patients exhibiting lower BCL2L10 expression did not demonstrate significantly favorable prognostic outcomes compared to those with higher BCL2L10 expression, characterized by (**A**) OS; (**B**) PFS; (**C**) DSS (both log-rank $p > 0.05$); (**D**) Prognostic evaluation based on BCL2L10 expression across various clinical features; (**E**) A nomogram derived from multivariate analysis incorporating clinical features linked to BCL2L10; (**F**) A calibration graph illustrating the model's predictive accuracy, as assessed through multivariable Cox regression method.

3.4. Assembling Protein–Protein Interaction Networks

Protein network analysis via STRING revealed BCL2L10-interacting partners implicated in HNSCC development, providing insights into its functional role in tumor biology. Analysis of research results shows the top six proteins along with their associated gene names, scores, including *BCL2L11, BIK, BCL2L2, UBQLN1, MCL1,* and *BECN1* (**Figure 5**).

A

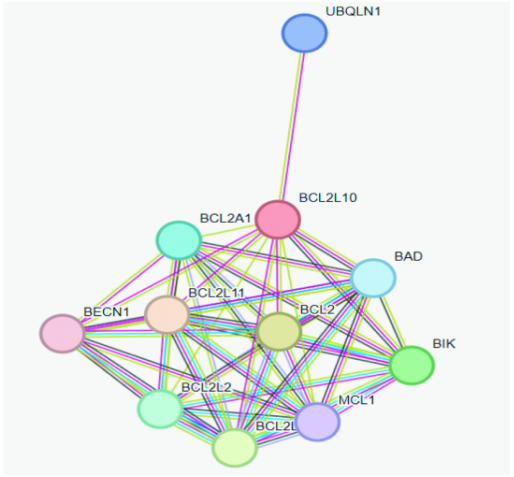

B

Gene symbol	Score
BIK	0.893
BCL2L2	0.88
BECN1	0.802
MCL1	0.805
UBQLN1	0.814
BCL2L11	0.993

Figure 5. BCL2L10-interacting proteins in HNSCC. (**A**) Proteins that bind to BCL2L10; (**B**) their co-expression values.

3.5. Whole-Transcriptome Association Study with BCL2L10 Expression

Transcriptomic profiling of BCL2L10 in HNSCC revealed significant associations with 295 downregulated and 473 upregulated genes (logFC > 1, adjusted $p < 0.05$; **Figure 6A**). A heatmap visualization highlighted the 14 most differentially expressed genes (DEGs, logFC > 2, padj < 0.01; **Figure 6B**). GO analysis identified female gamete generation as the predominant biological process linked to BCL2L10 activity (**Figure 6C**).

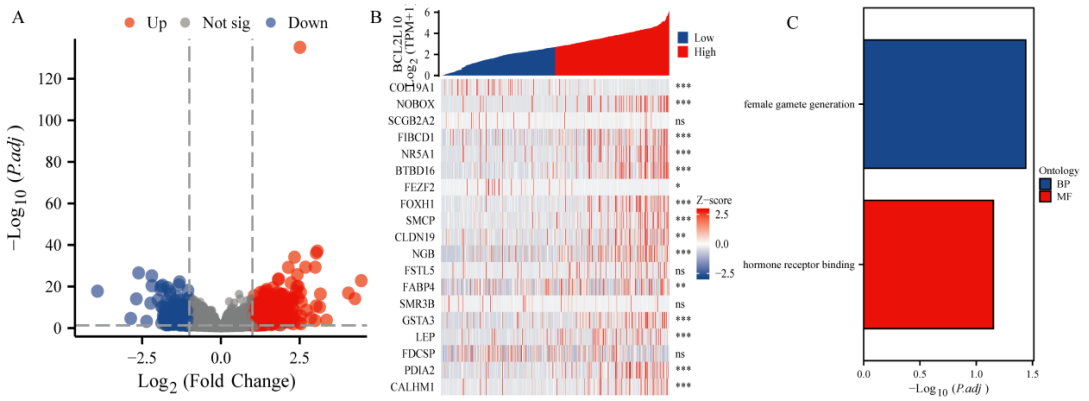

Figure 6. Analysis of *BCL2L10* gene expression and GO enrichment. (**A**) A volcano plot based on BCL2L10 highlights DEGs; (**B**) A heat map generated using BCL2L10 expression levels shows genes that were either upregulated or downregulated; (**C**) GO enrichment results of DEGs, filtered based on *BCL2L10* gene expression, were scrutinized using the metascape data repository.

3.6. Exploring BCL2L10 Expression through GSEA

TCGA-based GSEA revealed significantly enriched pathways (FDR < 0.25) when comparing BCL2L10 expression groups, with the top-ranked pathway identified by NES shown in **Figure 7**.

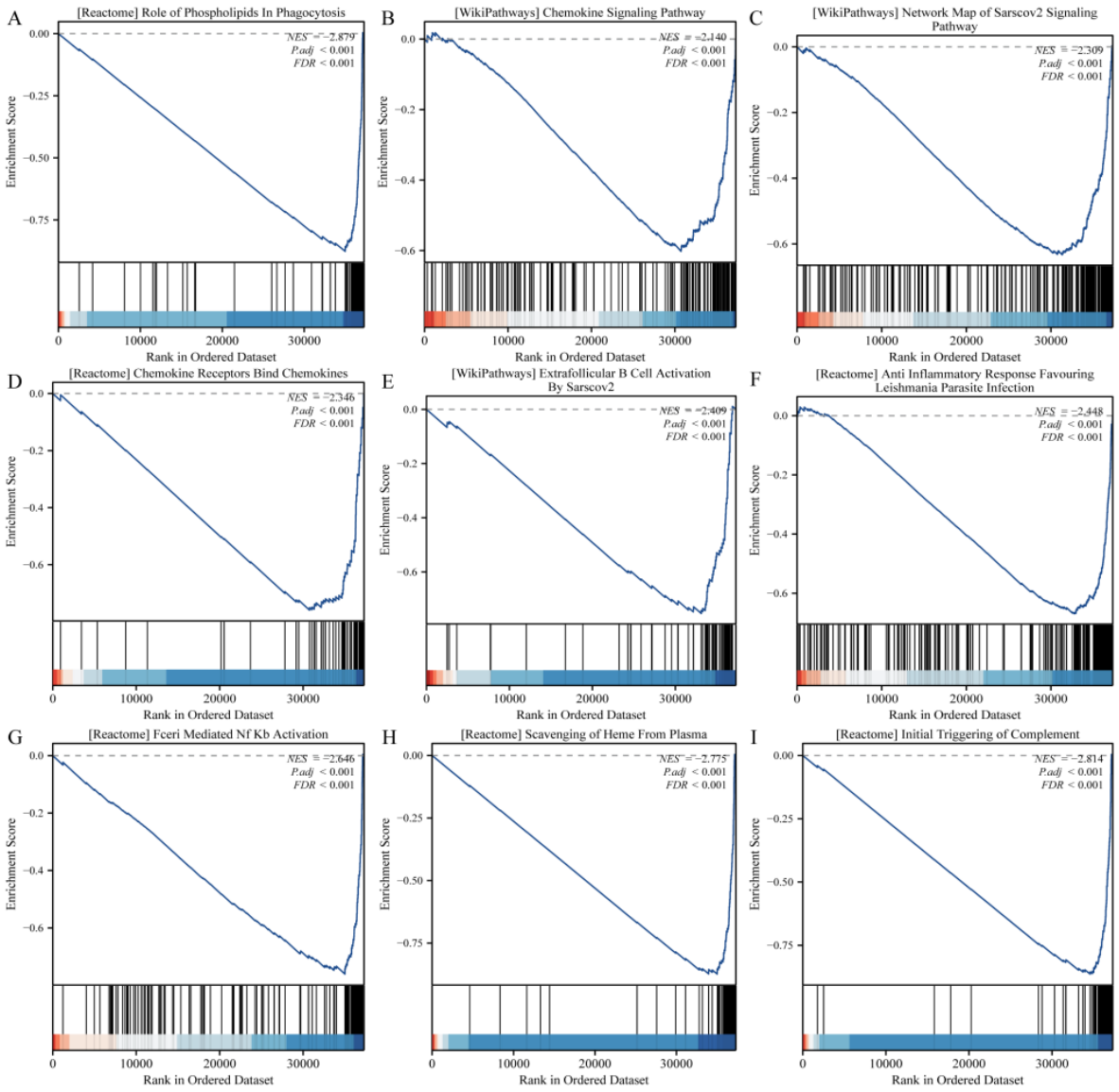

Figure 7. The insights of the GSEA. GSEA results showed that: (**A**) [reactome] role of phospholipids in phagocytosis; (**B**) [wikiPathways] chemokine signaling pathway; (**C**) [wikiPathways] network map of sarscov2 signaling pathway; (**D**) [reactome] chemokine receptors bind chemokines; (**E**) [wikiPathways] extrafollicular b cell activation by sarscov2; (**F**) [reactome] anti inflammatory response favouring leishmania parasite infection; (**G**) [reactome] fceri mediated nf kb activation; (**H**) [reactome] scavenging of heme from plasma; (**I**) [reactome] initial triggering of complement.

3.7. BCL2L10-Dependent Modulation of Immune Cell Recruitment in Tumor Tissues

Our investigation revealed significant immunogenomic associations between BCL2L10 expression and 24 immune cell populations in HNSCC. BCL2L10 demonstrated: (i) positive correlations with NK CD56bright cells, and (ii) negative correlations with pDC, TReg, CD8 T cells, and cytotoxic cells (**Figures 8A**, **8E–N**). Distinct BCL2L10 expression patterns were observed across various immune infiltrates, particularly in aDC, CD8 T cells, cytotoxic cells, macrophages, neutrophils, NK CD56dim cells, pDC, T cells, TReg, Th1 cells, TFH, and Tem (**Figures 8B–D**). The study found that the expression of most immune markers for various types of DCs, macrophages, neutrophils, NK cells, and T cells is associated with the level of *BCL2L10* gene expression in HNSCC.

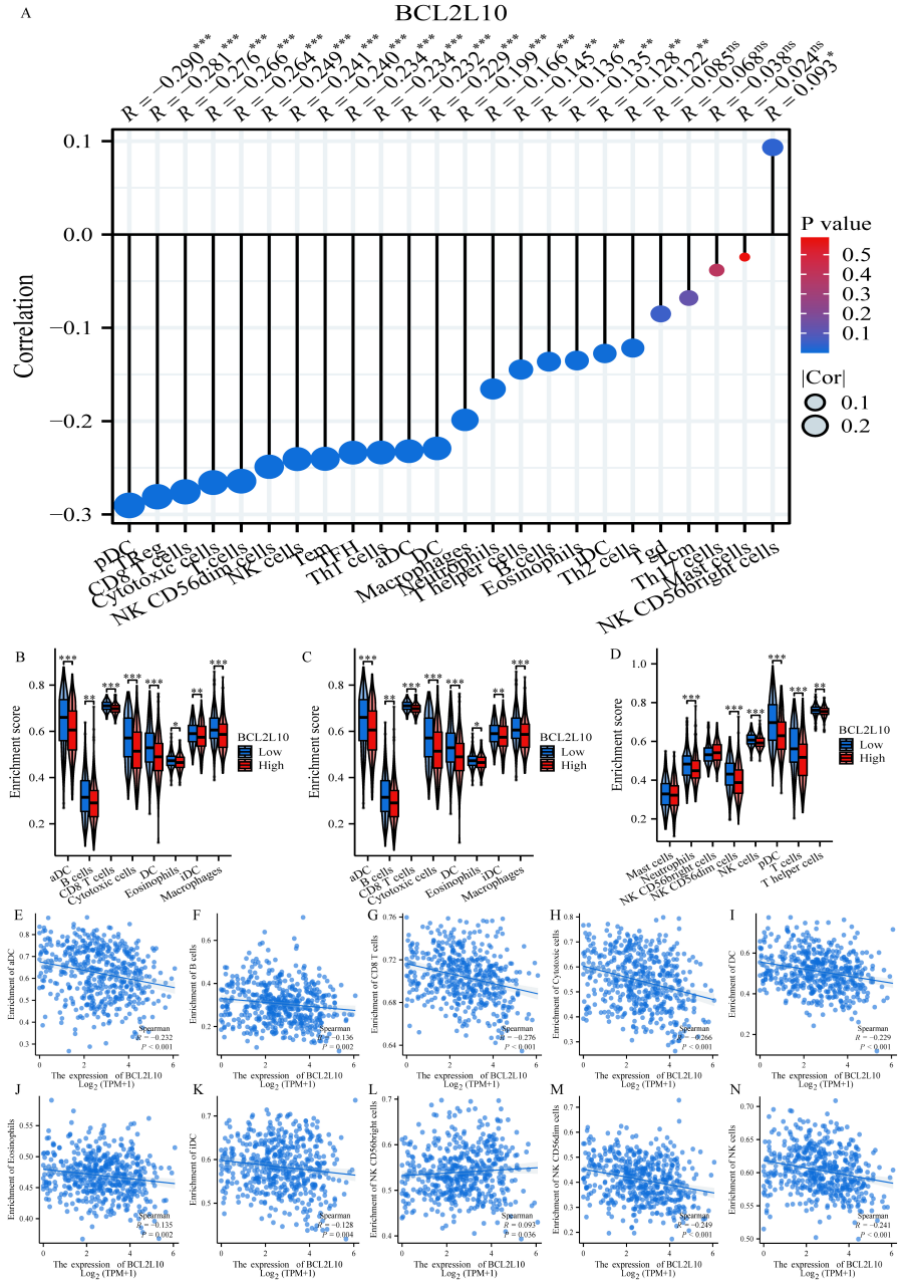

Figure 8. Correlation between BCL2L10 and immune cell invasion. (**A**) Analysis of the correlation between BCL2L10 expression and immune cell invasion profile; (**B–D**) Variations in the enrichment levels of specific immune cell subsets in groups with high and low *BCL2L10* gene expression; (**E–N**) Relationships between the *BCL2L10* gene expression and tumor microenvironment characteristics.

Note: *$p < 0.05$; **$p < 0.01$; ***$p < 0.001$. ns: no significance.

4. Discussion

The incidence of HNSCC shows significant regional and population differences. Its diagnosis mainly relies on histopathological examination combined with imaging assessment, but the rate of early diagnosis remains suboptimal [21]. In recent years, liquid biopsy technologies, such as circulating tumor DNA (ctDNA) testing, have provided new approaches for the early diagnosis and efficacy monitoring of HNSCC [22]. In terms of treatment, while the application of immune checkpoint inhibitors has significantly improved the prognosis for some patients, the overall response rate is only 15–20%, and there are significant individual differences [23]. The main challenges

in current HNSCC treatment include: treatment resistance due to tumor heterogeneity; treatment-related toxicity affecting patients' quality of life; and lack of reliable predictive biomarkers. The root causes of these issues lie in the complexity of the tumor microenvironment, including immune-suppressive cell infiltration, abnormal vasculature, and metabolic reprogramming. In particular, HPV-negative and smoking-related HNSCC show significantly poorer responses to existing treatments compared to HPV-positive tumors. Future research should focus on developing precise typing systems based on multi-omics and exploring new combined treatment strategies, such as the combination of immunotherapy and targeted therapy. These clinical realities highlight the urgent need for improved early detection methods and the development of more effective systemic therapies that should be tailored to tumor molecular characteristics [21–23]. Our investigation revealed significant associations between BCL2L10 expression and the progression of HNSCC. Utilizing Cox proportional hazards regression, we developed a prognostic stratification model that effectively categorized HNSCC patients into distinct risk groups. Notably, elevated BCL2L10 expression correlated with adverse clinical outcomes, as high-risk patients exhibited reduced survival rates. Univariate analyses confirmed BCL2L10 as a promising prognostic biomarker. These findings suggest that BCL2L10 may be useful in risk assessment and in developing personalized therapeutic strategies for HNSCC.

Ferroptosis, a novel iron-dependent programmed cell death mechanism, has garnered significant attention in cancer research in recent years. From a pathophysiological perspective, the occurrence of ferroptosis involves several key stages: first, dysregulation of intracellular iron metabolism leads to the accumulation of free iron; second, polyunsaturated fatty acids (PUFAs) undergo peroxidation under the action of lipoxygenases (LOXs); finally, the antioxidant defense system (especially the glutathione-GPX4 axis) is impaired. These changes collectively lead to the disruption of cell membrane integrity, abnormal mitochondrial morphology, and imbalance in redox homeostasis [11, 12]. Ferroptosis has multifaceted effects on cells. On one hand, it directly leads to the breakdown of the cell membrane system and dysfunction of organelles; on the other hand, damage-associated molecular patterns (DAMPs) released during ferroptosis can activate immune responses, making it potentially valuable for tumor immunotherapy. It is noteworthy that there are significant differences in the sensitivity of different tumor cells to ferroptosis, and these differences are closely related to the metabolic characteristics, antioxidant capacity, and iron metabolism status of tumor cells [24]. BCL2L10, as an atypical member of the BCL-2 protein family, has unique biological mechanisms. Unlike classical anti-apoptotic proteins, BCL2L10 not only functions by inhibiting the mitochondrial apoptosis pathway dependent on BAX/BAK but also forms complexes with various cell death regulatory proteins [14]. The latest research has found that BCL2L10 plays a dual role in regulating ferroptosis: in some tumors, BCL2L10 inhibits ferroptosis by stabilizing the GPX4 protein; under specific conditions, it can also promote ferroptosis, and this contradictory effect may be related to cell type and microenvironment factors [25]. In the field of tumor treatment, the regulation of the BCL2L10–ferroptosis axis shows broad application prospects. Multiple studies have shown that targeting BCL2L10 can significantly enhance the sensitivity of tumor cells to ferroptosis-inducing agents [26]. Our findings suggest that BCL2L10 may confer cytoprotective effects against ferroptosis in HNSCC, analogous to its established anti-apoptotic functions. The significantly elevated expression of BCL2L10 in tumor tissues compared to normal tissues (**Figures 1B–C**) suggests a potential role in evading iron-dependent cell death. Clinically, elevated BCL2L10 expression was correlated with reduced overall survival (**Figures 4A–C**), potentially indicating a selection advantage for tumor cells that resist iron toxicity. This aligns with the metabolic adaptation hypothesis, where BCL2L10-mediated GPX4 inhibition may decrease mitochondrial susceptibility to iron overload. The observed survival disparity may arise from two mechanisms: (1) direct iron detoxification through pathways regulated by BCL2L10, and (2) indirect metabolic reprogramming that promotes tumor persistence. These findings suggest that BCL2L10 could serve as both a clinical prognostic marker and a potential target for treatments aimed at modulating ferroptosis sensitivity in HNSCC.

Metabolic reprogramming is a key characteristic of tumor development and progression. Tumor cells alter their metabolic pathways to meet the energy demands and biosynthetic needs required for rapid proliferation. This metabolic reprogramming includes significant changes in lipid metabolism and iron metabolism, which together promote the malignant progression of tumors. It is noteworthy that different tumor types exhibit unique metabolic characteristics, which provides the possibility for developing tumor-specific treatment strategies [27]. Lipid metabolism plays multiple roles in tumor development and progression. On one hand, tumor cells enhance fatty acid synthesis and uptake to meet the demands of membrane synthesis and energy storage. On the other hand, lipid metabolites can act as signaling molecules to regulate the tumor microenvironment and metastasis process.

Notably, the crucial role of lipid peroxidation products in ferroptosis offers new avenues for targeted antitumor therapies that aim to modulate lipid metabolism [28]. Abnormal iron metabolism is another significant characteristic of tumors. Tumor cells increase iron uptake and storage by upregulating the expression of transferrin receptor and ferritin. Iron is not only an essential element for DNA synthesis and energy metabolism but also promotes tumor progression through the Fenton reaction, which generates reactive oxygen species. However, excessive iron can also induce ferroptosis, making iron metabolism regulation a crucial target for cancer treatment [29]. The interplay between lipid metabolism and tumor immunity is increasingly attracting attention. Lipid metabolic reprogramming in the tumor microenvironment significantly affects the function of immune cells. Lipid metabolites can directly regulate the expression of immune checkpoint molecules [30]. These findings offer new insights for developing tumor immunotherapies based on metabolic regulation. Our integrated multi-database analysis (GEO/TCGA/HPA) revealed markedly elevated BCL2L10 transcript levels in HNSCC specimens compared to normal controls. Clinically, patients with overexpression of BCL2L10 have shown significantly poorer survival outcomes, indicating its potential as both a diagnostic marker and a focus of clinical attention in the prognosis of HNSCC. This association remained significant even after adjusting for univariate factors.

Protein–protein interaction network analysis using STRING revealed BCL2L11, BCL2L2, and BIK as key functional partners of BCL2L10 in HNSCC. Members of the BCL2 protein family play crucial roles in regulating cell apoptosis and tumor development. BCL2L11, BCL2L2, and BIK are important members of this family, each with unique biological functions. BCL2L11 is a pro-apoptotic protein that induces mitochondrial outer membrane permeabilization by activating BAX/BAK, playing a key role in tumor suppression and chemosensitivity [31]. BCL2L2, on the other hand, has a strong anti-apoptotic function, promoting cell survival by inhibiting BAX/BAK activation, and is often overexpressed in various types of tumors. BIK, as a BH3-only protein, can neutralize anti-apoptotic proteins and directly activate BAX/BAK, although its pro-apoptotic activity is relatively weak [32]. The interaction between BCL2L10 and these proteins forms a complex regulatory network. Studies have shown that BCL2L10 can directly bind to BCL2L11 and inhibit its pro-apoptotic activity, which may be an important mechanism underlying the resistance of certain tumors to apoptosis-inducing therapies. Additionally, BCL2L10 exhibits a synergistic effect with BCL2L2, together forming a stronger anti-apoptotic complex that provides survival advantages to tumor cells. Notably, the interaction between BCL2L10 and BIK shows tissue specificity, promoting apoptosis in some types of tumors while inhibiting it in others [33]. These interactions have multiple impacts on tumorigenesis and cancer development. First, the imbalance of the BCL2L10–BCL2L11 axis leads to apoptosis escape, promoting tumor occurrence. Second, the synergistic effect of BCL2L10 and BCL2L2 enhances the survival ability of tumor cells, which is associated with poor prognosis. Additionally, the tissue-specific interaction between BCL2L10 and BIK may explain the differential responses of various tumors to apoptotic induction therapy [34,35]. Recent studies have also found that these interactions affect ferroptosis sensitivity, providing potential targets for developing new anti-tumor strategies [35]. These findings emphasize the therapeutic potential of targeting this regulatory axis, as BCL2L11/BIK/BCL2L2 regulators have shown promise in preclinical models of HNSCC. However, their interaction during HNSCC requires additional investigation. ROC curve analysis demonstrated moderate diagnostic potential for BCL2L10 in HNSCC (AUC = 0.654, 95% CI 0.591–0.717), supporting its utility as a putative biomarker. Elevated BCL2L10 expression correlated significantly with pathologic stage, clinical stage, histologic grade, and reduced overall survival. Gene ontology analysis further implicated BCL2L10 in female gamete generation pathways, highlighting its crucial role in oocyte maturation and fertilization processes.

The current prognostic evaluation in HNSCC primarily depends on conventional clinicopathological parameters, such as TNM staging, histological classification, and lymph node involvement status. The interplay between ferroptosis and the tumor immune microenvironment has become a new focus in cancer immunotherapy research. Recent studies have found that ferroptosis can significantly influence the infiltration pattern of tumor immune cells through various mechanisms. When tumor cells undergo ferroptosis, the released lipid peroxidation products and damage-associated molecular patterns (DAMPs) can promote the maturation and antigen presentation of dendritic cells (DCs), thereby enhancing the tumor infiltration and activation of CD8+ T cells. Additionally, glutamate release induced by ferroptosis can affect their antitumor function by modulating T cell metabolic reprogramming [36]. The molecular mechanisms of ferroptosis regulating immune infiltration involve multiple signaling pathways. On one hand, oxidized phospholipids released by ferroptotic cells can activate the TLR4/NF-κB pathway in macrophages, promoting their polarization towards the M1 type [37]. On the other hand, oxidized steroids accumulated during

ferroptosis can inhibit the immunosuppressive function of myeloid-derived suppressor cells (MDSCs) through LXR receptors. Notably, ferroptosis can also affect the efficacy of immune checkpoint blockade therapy by modulating PD-L1 expression [38]. However, the existing body of research on the relationship between the *BCL2L10* gene and immunocytes in HNSCC is insufficient. In this study, we innovatively explored the correlation between BCL2L10 expression in HNSCC and 24 distinct immune cell subtypes. Our results indicate that the expression of the *BCL2L10* gene is significantly and consistently correlated with the infiltration levels of NK CD56bright cells, pDC, TReg, CD8 T cells, and cytotoxic cells in HNSCC, underscoring its potential role in immune regulation within the tumor microenvironment. Research findings indicate that the expression levels of BCL2L10 are significantly associated with the infiltration characteristics of immune cells in tumor tissues. In various solid tumors, the overexpression of BCL2L10 is closely associated with reduced infiltration of CD8+ T cells, increased regulatory T cells (Tregs), and myeloid-derived suppressor cells (MDSCs). This alteration in immune cell composition directly leads to the formation of an immunosuppressive microenvironment, promoting tumor immune escape [39]. BCL2L10 has been confirmed to upregulate the expression of key immune checkpoint molecules through multiple pathways. Experimental data show that BCL2L10 can directly activate the transcription of PD-L1 and indirectly enhance the expression of CTLA-4 by stabilizing HIF-1α protein [40]. Additionally, BCL2L10 promotes the expression of co-inhibitory molecules such as TIM-3 and LAG-3 by activating the STAT3 signaling pathway [41]. These findings explain why tumors with high BCL2L10 expression have poor responses to immune checkpoint inhibitor therapy.

While this investigation provides valuable insights into BCL2L10's role in HNSCC, several limitations should be acknowledged. Our findings were derived primarily from retrospective bioinformatics analyses of public databases; the study lacks functional validation—future work should include in vitro assays and in vivo models to elucidate BCL2L10's mechanistic contributions to tumor progression, immune modulation, and tumor prognosis. Additionally, while we identified correlations between BCL2L10 and immune infiltration, the precise molecular pathways underlying these observations remain unexplored.

5. Conclusion

In summary, BCL2L10 upregulation in HNSCC may impact tumor progression and disease prognosis through pivotal molecular functions and pathways. Moreover, BCL2L10 expression correlates with the infiltration levels of various immune cell types. To bridge the gap between computational insights and clinical relevance, future work should employ laboratory experiments to validate BCL2L10's mechanistic contributions to HNSCC.

Author Contributions

Conceptualization, G.L. and Y.C.; methodology, X.X.; software, X.Y.; validation, Y.Z.; formal analysis, S.L.; investigation, X.Y.; resources, S.L.; data curation, S.L.; writing—original draft preparation, G.L.; writing—review and editing, Y.C.; visualization, X.X.; supervision, X.Y. All authors have read and agreed to the published version of the manuscript.

Funding

This work received no external funding.

Institutional Review Board Statement

Not applicable.

Informed Consent Statement

Not applicable.

Data Availability Statement

The data utilized in this study are accessible through online repositories. Details regarding the specific repository names and corresponding accession numbers are provided within the article.

Conflicts of Interest

The authors declare that there is no conflict of interest.

References

1. Johnson, D.E.; Burtness, B.; Leemans, C.R.; et al. Head and Neck Squamous Cell Carcinoma. *Nat. Rev. Dis. Primers* **2020**, *6*, 92. [CrossRef]
2. Ferris, R.L.; Blumenschein, G.; Fayette, J.; et al. Nivolumab for Recurrent Squamous-Cell Carcinoma of the Head and Neck. *N. Engl. J. Med.* **2016**, *375*, 1856–1867. [CrossRef]
3. Cohen, E.E.W.; Soulières, D.; Tourneau, C.L.; et al. Pembrolizumab Versus Methotrexate, Docetaxel, or Cetuximab for Recurrent or Metastatic Head-and-Neck Squamous Cell Carcinoma (KEYNOTE-040): A Randomised, Open-Label, Phase 3 Study. *Lancet Oncol.* **2019**, *303*, 156–167. [CrossRef]
4. Gillison, M.L.; Trotti, A.M.; Harris, J.; et al. Radiotherapy Plus Cetuximab or Cisplatin in Human Papillomavirus-Positive Oropharyngeal Cancer (NRG Oncology RTOG 1016): A Randomised, Multicentre, Non-Inferiority Trial. *Lancet* **2019**, *393*, 40–50. [CrossRef]
5. Whiteside, T.L. The Tumor Microenvironment and Its Role in Promoting Tumor Growth. *Oncogene* **2008**, *27*, 5904–5912. [CrossRef]
6. Seiwert, T.Y.; Fayette, J.; Cupissol, D.; et al. A Randomized, Phase II Study of Afatinib Versus Cetuximab in Metastatic or Recurrent Squamous Cell Carcinoma of the Head and Neck. *Ann. Oncol.* **2014**, *25*, 1813–1820. [CrossRef]
7. Schoenfeld, J.D.; Hanna, G.J.; Jo, V.Y.; et al. Neoadjuvant Nivolumab or Nivolumab Plus Ipilimumab in Untreated Oral Cavity Squamous Cell Carcinoma: A Phase 2 Open-Label Randomized Clinical Trial. *JAMA Oncol.* **2020**, *6*, 1563–1570. [CrossRef]
8. Lydiatt, W.M.; Patel, S.G.; Sullivan, B.; et al. Head and Neck Cancers—Major Changes in the American Joint Committee on Cancer Eighth Edition Cancer Staging Manual. *CA Cancer J. Clin.* **2017**, *67*, 122–137. [CrossRef]
9. Chow, L.Q.M.; Haddad, R.; Gupta, S.; et al. Antitumor Activity of Pembrolizumab in Biomarker-Unselected Patients with Recurrent and/or Metastatic Head and Neck Squamous Cell Carcinoma: Results From the Phase Ib KEYNOTE-012 Expansion Cohort. *J. Clin. Oncol.* **2016**, *34*, 3838–3845. [CrossRef]
10. Gillison, M.L.; Akagi, K.; Xiao, W.; et al. Human Papillomavirus and the Landscape of Secondary Genetic Alterations in Oral Cancers. *Genome Res.* **2019**, *29*, 1–17.
11. Chen, X.; Kang, R.; Kroemer, G.; et al. Broadening Horizons: The Role of Ferroptosis in Cancer. *Nat. Rev. Clin. Oncol.* **2021**, *18*, 280–296. [CrossRef]
12. Jiang, X.; Stockwell, B.R.; Conrad, M. Ferroptosis: Mechanisms, Biology and Role in Disease. *Nat. Rev. Mol. Cell Biol.* **2021**, *22*, 266–282. [CrossRef]
13. Lei, G.; Zhuang, L.; Gan, B.; et al. Targeting Ferroptosis as a Vulnerability in Cancer. *Nat. Rev. Cancer* **2022**, *22*, 381–396. [CrossRef]
14. Wu, Y.; Chen, K.; Li, L.; et al. Plin2-Mediated Lipid Droplet Mobilization Accelerates Exit From Pluripotency by Lipidomic Remodeling and Histone Acetylation. *Cell Death Differ.* **2022**, *29*, 934–947. [CrossRef]
15. Li, H.; Jiang, W.; Zhang, S.R.; et al. The Platelet Pannexin 1–IL-1β Axis Orchestrates Pancreatic Ductal Adenocarcinoma Invasion and Metastasis. *Oncogene* **2023**, *42*, 1123–1135. [CrossRef]
16. Wang, X.; Shi, Y.; Shi, H.; et al. MUC20 Regulated by Extrachromosomal Circular DNA Attenuates Proteasome Inhibitor Resistance of Multiple Myeloma by Modulating Cuproptosis. *J. Exp. Clin. Cancer Res.* **2024**, *43*, 68. [CrossRef]
17. Babuharisankar, A.P.; Kuo, C.L.; Chou, H.Y.; et al. Mitochondrial Lon-Induced Mitophagy Benefits Hypoxic Resistance via Ca^{2+}-Dependent FUNDC1 Phosphorylation at the ER–Mitochondria Interface. *Cell Death Dis.* **2023**, *14*, 199. [CrossRef]
18. Liu, J.; Kuang, F.; Kroemer, G.; et al. Autophagy-Dependent Ferroptosis: Machinery and Regulation. *Cell Chem. Biol.* **2020**, *27*, 420–435. [CrossRef]
19. Yang, W.S.; Kim, K.J.; Gaschler, M.M.; et al. Peroxidation of Polyunsaturated Fatty Acids by Lipoxygenases Drives Ferroptosis. *Proc. Natl. Acad. Sci.* **2016**, *113*, E4966–E4975. [CrossRef]
20. Tao, W.; Yufeng, L.; Qing, L.; et al. Cuproptosis-Related Gene FDX1 Expression Correlates with the Prognosis and Tumor Immune Microenvironment in Clear Cell Renal Cell Carcinoma. *Front. Immunol.* **2022**, *13*, 999823. [CrossRef]
21. Leemans, C.R.; Braakhuis, B.J.; Brakenhoff, R.H. The Molecular Biology of Head and Neck Cancer. *Nat. Rev. Cancer* **2011**, *11*, 9–22. [CrossRef]

22. Hanna, G.J.; Lizotte, P.; Cavanaugh, M.; et al. Frameshift Events Predict Anti-PD-1/L1 Response in Head and Neck Cancer. *JCI Insight* **2018**, *3*, e98811. [CrossRef]
23. Liu, X.; Harbison, R.A.; Varvares, M.A.; et al. Immunotherapeutic Strategies in Head and Neck Cancer: Challenges and Opportunities. *J. Clin. Invest.* **2025**, *135*, e188128. [CrossRef]
24. Jiang, M.; Qiao, M.; Zhao, C.; et al. Targeting Ferroptosis for Cancer Therapy: Exploring Novel Strategies From Its Mechanisms and Role in Cancers. *Transl. Lung Cancer Res.* **2020**, *9*, 1569–1584. [CrossRef]
25. Xu, R.; Peng, H.; Yang, N.; et al. Nuclear lncRNA CERNA1 Enhances Cisplatin-Induced Cell Apoptosis and Overcomes Chemoresistance via Epigenetic Activation of BCL2L10 in Ovarian Cancer. *Genes Dis.* **2023**, 10, 10–13. [CrossRef]
26. Wen, Z.; Pei, B.; Dai, L.; et al. Risk Factors Analysis and Survival Prediction Model Establishment of Patients With Lung Adenocarcinoma Based on Different Pyroptosis-Related Gene Subtypes. *Eur. J. Med. Res.* **2023**, *28*, 601. [CrossRef]
27. Martinez-Reyes, I.; Chandel, N.S. Cancer Metabolism: Looking Forward. *Nat. Rev. Cancer* **2021**, *21*, 669–680. [CrossRef]
28. Currie, E.; Schulze, A.; Zechner, R.; et al. Cellular Fatty Acid Metabolism and Cancer. *Cell Metab.* **2013**, *18*, 153–161. [CrossRef]
29. Alqarihi, A.; Kontoyiannis, D.P.; Ibrahim, A.S. Mucormycosis in 2023: An Update on Pathogenesis and Management. *Front. Cell. Infect. Microbiol.* **2023**, *13*, 1254919. [CrossRef]
30. Yang, K.; Wang, X.; Song, C.; et al. The Role of Lipid Metabolic Reprogramming in the Tumor Microenvironment. *Theranostics.* **2023**, *13*, 1774–1808. [CrossRef]
31. Willis, S.; Day, C.L.; Hinds, M.G.; et al. The BCL-2-Regulated Apoptotic Pathway. *J. Cell Sci.* **2003**, *116*, 4053–4056. [CrossRef]
32. Osterlund, E.J.; Hirmiz, N.; Nguyen, D.; et al. Endoplasmic Reticulum Protein BIK Binds to and Inhibits Mitochondria-Localized Antiapoptotic Proteins. *J. Biol. Chem.* **2023**, *299*, 102863. [CrossRef]
33. Quezada, M.J.; Picco, M.E.; Villanueva, M.B.; et al. BCL2L10 Is Overexpressed in Melanoma Downstream of STAT3 and Promotes Cisplatin and ABT-737 Resistance. *Cancers* **2021**, *13*, 78. [CrossRef]
34. Lee, S.Y.; Kwon, J.; Lee, K.A. BCL2L10 Induces Metabolic Alterations in Ovarian Cancer Cells by Regulating the TCA Cycle Enzymes SDHD and IDH1. *Oncol Rep.* **2021**, *45*, 47. [CrossRef]
35. Chen, L.; Ning, J.; Linghu, L.; et al. USP13 Facilitates a Ferroptosis-to-Autophagy Switch by Activation of the NFE2L2/NRF2–SQSTM1/p62–KEAP1 Axis Dependent on the KRAS Signaling Pathway. *Autophagy* **2025**, *21*, 565–582. [CrossRef]
36. Yang, Y.; Wang, Y.; Guo, L.; et al. Interaction Between Macrophages and Ferroptosis. *Cell Death Dis.* **2022**, *13*, 355. [CrossRef]
37. Hao, X.; Zheng, Z.; Liu, H.; et al. Inhibition of APOC1 Promotes the Transformation of M2 Into M1 Macrophages via the Ferroptosis Pathway and Enhances Anti-PD1 Immunotherapy in Hepatocellular Carcinoma Based on Single-Cell RNA Sequencing. *Redox Biol.* **2022**, *56*, 102463. [CrossRef]
38. Yu, Y.; Huang, X.; Liang, C.; et al. Evodiamine Impairs HIF1A Histone Lactylation to Inhibit Sema3A-Mediated Angiogenesis and PD-L1 by Inducing Ferroptosis in Prostate Cancer. *Eur. J. Pharmacol.* **2023**, *957*, 176007. [CrossRef]
39. Xu, W.; Li, Y.; Liu, L.; et al. Icaritin-Curcumol Activates $CD8^+$ T Cells Through Regulation of Gut Microbiota and the DNMT1/IGFBP2 Axis to Suppress the Development of Prostate Cancer. *J. Exp. Clin. Cancer Res.* **2024**, *43*, 149. [CrossRef]
40. Chiu, K.; Bashir, S.T.; Nowak, R.A.; et al. Subacute Exposure to Di-Isononyl Phthalate Alters the Morphology, Endocrine Function, and Immune System in the Colon of Adult Female Mice. *Sci. Rep.* **2020**, *10*, 18788. [CrossRef]
41. Liu, F.; Pan, R.; Ding, H.; et al. UBQLN4 Is an ATM Substrate That Stabilizes the Anti-Apoptotic Proteins BCL2A1 and BCL2L10 in Mesothelioma. *Mol. Oncol.* **2021**, *15*, 3738–3752. [CrossRef]